Synthesis and Crystal Structure of a New Vanadyl Phosphate $[H_{0.6}(VO)_3(PO_4)_3(H_2O)_3]\cdot 4H_2O$ and Its Conversion to Porous Products

Boris G. Shpeizer, Xiang Ouyang, Joy M. Heising, and Abraham Clearfield*

Department of Chemistry, Texas A&M University, College Station, Texas 77843-3012

Received November 9, 2000. Revised Manuscript Received April 2, 2001

Yellow layered $VOPO_4\cdot 2H_2O$ was found to spontaneously, but slowly, convert to a green phase $[H_{0.6}(VO)_3(PO_4)_3(H_2O)_3]\cdot 4H_2O$ upon standing in air. This phase could be prepared hydrothermally from $V_2O_5 + H_3PO_4$ with a small amount of reducing agent added. Single-crystal X-ray analysis gave $a = 7.371(3)$ Å, $b = 26.373(11)$ Å, $c = 8.827(4)$ Å, $\beta = 106.777(7)°$, space group $P2_1/c$, and $Z = 4$. The two vanadyl phosphates are related because the c axis of the green phase is $\sqrt{2}\cdot a$ where a is the a-unit cell dimension of the yellow tetragonal $VOPO_4\cdot 2H_2O$ and the b axis is $\sqrt{2}\cdot 3a$. The green phase was found to intercalate approximately 2 mol of alkylamines/vanadium. A modified gel technique based upon mixtures of amine-intercalated vanadyl phosphate and nickel acetate were utilized to obtain microporous products with nickel polymers. Surface areas as high as 400 m^2/g were obtained with pore diameters of 10 to as large as 23 Å. The pore size depended upon the nature of the alcohol solvent, the size of the amine used to enlarge the interlayer space, and the temperature of calcination.

Introduction

Vanadium phosphates have been extensively investigated by a diverse group of scientists in recent years due to their catalytic activity.[1] Of particular interest is $VOPO_4\cdot 2H_2O$, a layered compound that can undergo intercalation reactions. A variety of guest species, including pyridine[2], aniline[3], amides,[4] amines,[5] carboxylic acids,[6] and alcohols and diols[7] have been inserted between the layers by the displacement of a coordinated water molecule. Other guest species, such as alkylammonium ions,[8] alkali metal cations,[9] transition metal cations,[10,11] and ferrocene[12] have been intercalated through partial or complete reduction of the vanadium atoms to V(IV) in the host structure. Recently, a mesostructured oxovanadium phosphate has been synthesized from a V_2O_5, H_3PO_4 mixture in acid solution using cetyltrimethylammonium ion as a template.[13]

Our interest in the vanadyl phosphates stems from the possibility of pillaring them to create porous vanadyl derivatives with potential as catalysts and unusual magnetic behavior. The route to obtain inorganically pillared products may lie through exfoliation or intercalation of loosely held guest species to spread the layers apart.[14] In our efforts to synthesize $VOPO_4\cdot 2H_2O$ for intercalation reactions, we isolated lamellar crystalline vanadium phosphates that are yellow, light green, and dark green using very similar synthetic conditions and investigated the structural relationship between these phases. We were then able to synthesize several types of porous materials that are described in this report.

Experimental Section

Yellow $VOPO_4\cdot 2H_2O$. The method used was a modification of the procedure developed by Ladwig.[5a] V_2O_5 (Johnson Matthey, 2.4 g, 13.2 mmol) was weighed into a 110-mL Teflon liner, followed by addition of 46.8 g of deionized H_2O (2.6 mol), 24 g of 85% H_3PO_4 (EM Science, 0.208 mol), and 2.3 g of 70% HNO_3 (EM Science, 25.6 mmol). The mixture was then stirred (V:HNO_3:H_3PO_4:H_2O ratio was 1:0.97:7.9:98.5) until it became homogeneous (30 min to 1 h). The liner was then placed in a steel hydrothermal bomb and heated at 130 °C for 8−32 h.

(1) Centi, G.; Trifiró, F.; Ebner, J. R.; Franchetti, V. M. *Chem. Rev.* **1988**, *88*, 55. (b) Garbassi, F.; Bart, J. C. J.; Montino, F.; Petrini, G. *Appl. Catal.* **1985**, *16*, 271. (c) Guiliants V. V.; Benziger, J. B.; Sundaresan, S. *Catalysis* **1996**, *101*, 991.

(2) Johnson, J. W.; Jacobson, A. J.; Brody, J. F.; Rich, S. M. *Inorg. Chem.* **1982**, *21*, 3820.

(3) Kinomura, N.; Toyama, T.; Kumada, N. *Solid State Ionics* **1995**, *78*, 281.

(4) Martinez-Lara, M.; Moreno-Real, L.; Jimenez-Lopez, A.; Bruque-Gamez, S.; Rodriguez-Garcia, A. *Mater. Res. Bull.* **1986**, *21*, 13.

(5) Ladwig, G. Z. *Anorg. Allg. Chem.* **1965**, *338*, 266. (b) Beneš, L.; Hyklová, R.; Kalousová, J.; Votinský, J. *Inorg. Chim. Acta* **1990**, *177*, 71.

(6) Beneš, L.; Votinský, J.; Kalousová, J.; Handlíř, K. *Inorg. Chim. Acta* **1990**, *176*, 255.

(7) Beneš, L.; Melánová, K.; Zima, V.; Kalousová, J.; Votinský, J. *Inorg. Chem.* **1997**, *36*, 2850.

(8) Martinez-Lara, M.; Jimenez-Lopez, A.; Moreno-Real, L.; Bruque-Gamez, S.; Casal, B.; Ruiz-Hitzky, E. *Mater. Res. Bull.* **1985**, *20*, 549.

(9) Johnson, J. W.; Jacobson, A. J. *Angew. Chem., Int. Ed. Engl.* **1983**, *22*, 412. (b) Ayyappan, P. Ph.D. Dissertation, Indian Institute Technology, Delhi, India, Sept 1999; p 24 and references therein.

(10) Jacobson, A. J.; Johnson, J. W.; Brody, J. F.; Scanlon, J. C.; Lewandowski, J. T. *Inorg. Chem.* **1985**, *24*, 1782.

(11) Antonio, M. R.; Barbour, R. L.; Blum, P. R. *Inorg. Chem.* **1987**, *26*, 1235.

(12) Rodríguez-Castellón, E.; Jiménez-Lopéz, A.; Martínez-Lara, M.; Moreno-Real, L. *J. Incl. Phenom.* **1987**, *5*, 335.

(13) El Haskouri, J.; Cabrera, S.; Roca, M.; Alamo, J.; Beltrán-Porter, A.; Beltrán-Porter, D.; Marcos, M. D.; Amorós, P. *Inorg. Chem.* **1999**, *38*, 4243.

(14) Clearfield, A.; Roberts, B. D. *Inorg. Chem.* **1988**, *27*, 3237. (b) Olivera-Pastor, P.; Maireles-Torres, P.; Rodríguez-Castellón, E.: Jiménez-Lopéz, A. *Chem. Mater.* **1996**, *8*, 1758.

10.1021/cm0008821 CCC: $20.00
Published on Web 06/09/2001

The product was bright yellow solid, but because it slowly turned green with time, once it was isolated, the crystals were stored in the mother liquor of the reaction. A portion of the crystals was isolated by filtration, rinsed with a little water and/or ethyl acetate, and dried in an oven at 75 °C for about 10 min prior to characterization.

Light Green $VOPO_4\cdot 2H_2O$. V_2O_5 (5.32 g, 29.2 mmol) was weighed into a 110-mL Teflon liner, followed by 53.2 g of deionized H_2O (2.95 mol) and 26.8 g of 85% H_3PO_4 (0.232 mol) ($V:H_2PO_4:H_2O$ ratio was 1:4:≈50), and then stirred until it became homogeneous. The liner was then placed in a steel hydrothermal bomb and heated for 1 week at temperatures ranging in different runs from 130 to 195 °C. The product was isolated by filtration. Initially, the samples were rinsed with ethanol, but it became clear that the products could undergo reaction with residual ethanol over time; hence, they were rinsed in the same manner as the yellow product.

Dark Green $H_xVOPO_4\cdot 2.33H_2O$. V_2O_5 (5.32 g, 29.2 mmol) was weighed into a 110-mL Teflon liner, followed by the addition of 53.2 g of deionized H_2O (2.95 mol), 26.8 g of 85% H_3PO_4 (0.232 mol), and 0.2 mL of ethanol (2.4 mmol) ($V:EtOH:H_3PO_4:H_2O$ ratio was 1:0.041:3.97:50.5), and then stirred until it became homogeneous. The liner was then placed into a steel hydrothermal bomb and heated at temperatures ranging from 130 to 195 °C for 1 week. The isolation of the product was analogous to that used for the light green product.

Amine Intercalates. The vanadium phosphate was reacted with excess alkylamines (3−4:1) in ethanol (or ethyl acetate) for several hours up to 2 days. Bluish white products formed, which were isolated by filtration, rinsed with ethanol, and dried.

Porous Products Based on Nickel Acetate. An alcohol solution of the dark green vanadyl phosphate, nickel acetate, and hexylamine was vigorously stirred for 1 h. To this mixture was added a highly diluted solution of water in ethanol, all the while being stirred vigorously. This procedure resulted in the formation of a gel, which was refluxed, and the solid was separated from the mother liquor. The solid was then washed in ethanol and dried at 60−65 °C at ambient pressure. An example of this procedure follows: 7.2 g (0.0348 mol) of the dark green vanadyl phosphate (empirical formula $H_xVOPO4\cdot 2.33H_2O$), 12.4 g of nickel acetate tetrahydrate (0.0498 mol), and 19 g of hexylamine (0.188 mol) were dissolved in respectively methanol, propanol, or heptanol and stirred for 1 h. Addition of a mixture of water and alcohol (1:3) resulted in the formation of the gel. The gel was refluxed for 10−15 h and the solid recovered by filtration. The solid was dried at 60−65 °C.

Characterization. Powder X-ray diffraction patterns of samples were initially measured using a Scintag PAD V powder X-ray diffractometer with Ni-filtered Cu Kα radiation. Higher quality patterns were obtained using a Rigaku-RU200B rotating anode X-ray powder diffractometer using Cu Kα radiation with a graphite monochromator. Samples were ground and packed into a sample holder or loaded into an aerosol chamber and embedded on glass fiber filter paper (Whatman GF/C 4.25 cm) to reduce preferred orientation. Electron paramagnetic resonance (EPR) spectra of the finely ground powders were recorded at room temperature using a Bruker ESP 300 spectrometer. Thermogravimetric analyses were collected on a DuPont Thermal Analyst 2000 at heating rates of 1−10 °C/min under flowing N_2 (30−40-mL flow rate) or O_2. FTIR spectra of finely ground samples were measured in diffuse reflectance mode on a Perkin-Elmer 2000 FTIR spectrometer at a resolution of 2 or 4 cm^{-1}, gain 4, and OPD (optical path difference) velocity 2 cm/s. Some spectra were obtained using KBr disks on a Biorad FTS-40 spectrophotometer. Elemental analyses were obtained from Galbraith Laboratories, Inc., Knoxville, TN. For metal analyses, the samples were digested in aqueous HF solutions and analyzed with a SpectraSpan VI DCP, Applied Research Laboratories, operating with AdaM VI Software, Interface Design, Inc. Surface area measurements were performed on an Autosorb-6 (Quantachrome) unit using nitrogen absorption at liquid nitrogen temperature. Both pure N_2 as an absorbate and N_2 in He as a carrier gas were utilized. Precalcined samples were outgassed at 200−390 °C. The resulting experimental data were analyzed using the software supplied by Quantachrome Corp. and surface areas were calculated on the basis of the BET model. Solid-state MAS NMR spectra of the samples were measured at room temperature on a Bruker MSL 300 operating at 300 MHz with a MAS rate of ≈5 kHz. 85% H_3PO_4 was used as a ^{31}P reference.

Crystal Structure Data Collection. Exceedingly small platelet type crystals were isolated from the dark green vanadyl phosphate preparation. Data collection was carried out on a Bruker SMART 1000 CCD Platform diffractometer equipped with monochromated Mo Kα radiation and an Oxford Cold Stream low-temperature controller. Data collection and reduction were performed with SMART5.0[15] and SAINT-PLUS6.0[16] from Bruker AXS. Twinned crystal data indexing and deconvolution were performed with GEMINI1.0 from Bruker AXS.[17] Crystallographic computing was performed on a Pentium 450-MHz personal workstation using the SHELXTL 5.10 package[18] from Bruker AXS. Data merging and absorption correction were performed with XPREP[18] from Bruker AXS.

A dark-greenish platelet crystal **(1)** of approximate dimensions 0.18 × 0.18 × 0.01 mm^3 was mounted on the tip of a glass fiber with Dow Corning silicone grease. Preliminary cell parameters were obtained from the indexing and refinement of 15 reflections from 60 frames with an exposure time of 10 s/frame. Unit cell parameters indicated a monoclinic system with $a = 7.36(2)$ Å, $b = 26.39(6)$ Å, $c = 8.84(2)$ Å, $\beta = 106.9(2)°$, and $V = 1643(5)$ $Å^3$. A full sphere of data with 2474 frames was collected with a scan width of 0.3° in ω and an exposure time of 20 s/frame at −100 °C. Re-indexing a reflection list of 871 strong reflections with the GEMINI1.0 program[17] indicated the presence of rotational twins, which corresponded to 568 independent reflections for component A and 80 independent reflections for component B. The remainder of the 211 reflections could be indexed to both components. Twinned component B could be transformed to component A by rotating 180° around the $(00\bar{1})$ c axis in direct space or $(\bar{1}00)$ in reciprocal space. The twinning law is $[-1\ 0\ -1/2,\ 0\ \bar{1}\ 0,\ 0\ 0\ 1]$. The data were integrated by using the orientation matrix of component A with the SAINT PLUS package[16] Laue crystal symmetry constraints. Final cell parameters were obtained by refining the *xyz* centroids of 1979 strong reflections with $I/\sigma > 10$. The unit cell parameters were determined to be $a = 7.371(3)$ Å, $b = 26.373(11)$ Å, $c = 8.827(4)$ Å, $\beta = 106.777(7)°$, and $V = 1642.9(12)$ $Å^3$. A semiempirical absorption correction (lamina mode) was performed with XPREP[18] and led to a transmission parameter between 1 and 0.435. Redundant reflections were merged and truncated to a maximum 2-Å angle of 49.42°, with 9668 total reflections in the range of $-8 \le h \le 8$, $-31 \le k \le 31$, $-10 \le l \le 10$, and $R_{int} = 0.0733$. A total of 2799 unique reflections were used in structure solution and refinement. The final reliability indices were $R_1 = 7.6\%$ and $wR_2 = 19.0\%$ for 1898 reflections with $I > 2\sigma$. A search for untwinned crystals was fruitless.

Structure Solution and Refinement

Structure solution and refinement were performed with the SHELXTL 5.10 package[18] in space group $P2_1/c$ (#14). The positions of all the non-hydrogen atoms were located by direct methods and refined by full-matrix least squares on F^2. Disordered positions of lattice water

(15) SMART Version 5.0, Area-Detector Instrument Control and Data Acquisition Software, Bruker AXS Inc., Madison, WI.

(16) SAINT PLUS Version 6.01, 6/22/99. Area-Detector Data Integration Software, Bruker AXS Inc., Madison, WI, 1999.

(17) GEMINI (TWINNING 2.0) Version 1.0, 10/1/99. Auto-Indexing Program for Twinned Crystals, Bruker AXS Inc., Madison, WI, 1999.

(18) SHEXTL (XPREP, XS, XL and XP) Version 5.10, 10/29/98. Structure Solution and Refinement Package, Bruker AXS, Madison, WI, 1998.

Table 1. Crystal Data and Structure Refinement for $[H_{0.6}(VO)_3(PO_4)_3(H_2O)_3]\cdot 4H_2O$

formula (FW)	$V_3P_3H_{14.6}O_{22}$ (612.45)
temperature	173(2) K
wavelength	0.71073 Å
crystal system	monoclinic
space group	$P2_1/c$
unit cell dimensions	$a = 7.371(3)$ Å, $\alpha = 90°$
	$b = 26.373(11)$ Å, $\beta = 106.777(7)°$
	$c = 8.827(4)$ Å, $\gamma = 90°$
volume	1642.9(12) Å^3
Z	4
density (calculated)	2.476 Mg/m^3
absorption coefficient	2.083 mm^{-1}
crystal size	0.18 × 0.18 × 0.01 mm^3
θ range for data collection	1.54°−24.71°
reflections collected	9668
independent reflections	2799 [$R_{(int)} = 0.0733$]
absorption correction	semiempirical
max. and min. transmission	1.0000 and 0.4350
data/restraints/parameters	2799/1/261
goodness-of-fit on F^2	1.076
final R indices [$I > 2\sigma(I)$]	$R_1 = 0.0765$, $wR_2 = 0.190$
R indicies (all data)	$R_1 = 0.1010$, $wR_2 = 0.2024$
largest diff. peak and hole	0.700 and −0.801 e·Å^{-3}

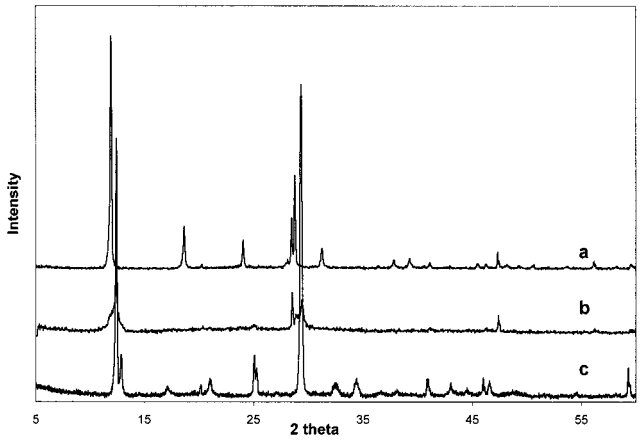

Figure 1. X-ray powder diffraction patterns of the (a) yellow, (b) light green, and (c) dark green vanadyl phosphate phases.

molecules were located from a difference map. Two disordered lattice water molecules were modeled and refined to 0.36/0.64 occupancies in two positions. One disordered water molecule was modeled over four positions and the occupancies were refined to the summation of 1. All non-hydrogen atoms were refined anisotropically except the disordered lattice water molecules, which were refined isotropically. Hydrogen atoms were placed in idealized positions. Crystallographic data for **1** are summarized in Table 1.

Results

Powder X-ray diffraction patterns for the three phases, Figure 1, have similar yet distinct characteristics. The bright yellow phase X-ray pattern identifies it as $VOPO_4\cdot 2H_2O$, whose structure is known.[19,20] The 001 reflection, at $d = 7.44$ Å, corresponds to the interlayer separation. The light green product gives rise to a pattern with very few peaks, indicating that the material exhibits severe preferred orientation, and even those peaks are rather weak when $l > 2$. It appears to be layered, with a d spacing comparable to that of the yellow compound; however, there is an additional peak in close proximity to the 001 reflection ($d \sim 7.2$ Å). The layered nature of these phases, as demonstrated by the XRD patterns, is also evident from the SEM pictures, even at magnification as low as 500×.

Table 2. Selected Bond Lengths (Å) and Angles (deg) for $[H_{0.6}(VO)_3(PO_4)_3(H_2O)_3]\cdot 4H_2O$

Bond Lengths			
V1−O1	1.967(7)	V2−O6	1.905(6)
V1−O2	1.962(7)	V2−O7	1.896(6)
V1−O3	1.955(7)	V2−O8	1.908(7)
V1−O4	1.967(7)	V2−O9	1.916(7)
V1−O5	1.540(7)	V2−O10	1.538(7)
V1−O1W	2.213(7)	V2−O2W	2.281(8)
V3−O11	1.924(7)	V3−O14	1.914(7)
V3−O12	1.914(7)	V3−O15	1.536(8)
V3−O13	1.948(7)	V3−O3W	2.226(9)

Angles			
O1−V1−O2	88.3(3)	O5−V1−O1	99.7(3)
O1−V1−O3	161.5(3)	O5−V1−O2	99.2(4)
O1−V1−O4	88.9(3)	O5−V1−O3	98.8(3)
O2−V1−O3	89.9(3)	O5−V1−O4	98.1(3)
O2−V1−O4	162.6(3)	O1W−V1−O1	79.9(3)
O3−V1−O4	87.4(3)	O1W−V1−O2	81.7(3)
O5−V1−O1W	179.0(3)	O1W−V1−O3	81.6(3)
		O1W−V1−O4	80.9(3)

The dark green phase is also lamellar, with a slightly smaller interlayer separation (7.12 Å) relative to the yellow phase (7.44 Å). Like the light green phase, there is an additional peak at $d = 6.89$ Å. The diffraction pattern from the dark green phase appears to contain more reflections, suggesting that the crystals are better formed than the light green phase.

Single-Crystal X-ray Analysis, Dark Green $H_xVOPO_4\cdot 2.33H_2O$. The structure is layered and consists of vanadyl cations linked to each other through corner sharing with four phosphate groups. A water molecule completes the octahedral coordination of the vanadium atom. The arrangement of octahedra and tetrahedra are shown in Figure 2. The b axis is slightly more than 26 Å in length and is puckered, resembling a sinusoidal wave function. There are three unique vanadium atoms per unit cell; each appears to have a V═O bond distance of ≈1.54(1) Å, comparable to the distance observed in tetragonal $VOPO_4\cdot 2H_2O$. The V−OH_2 distances are between 2.21(1) and 2.28(1) Å (Table 2) (compared to 2.23 Å in tetragonal $VOPO_4\cdot 2H_2O$). The equatorial V−O distances are ≈1.90 Å in tetragonal $VOPO_4\cdot 2H_2O$ but range from 1.90 to 1.97 Å in the dark green phase. Interestingly, the V1−O bonds average 1.963 Å and are larger than the same bond lengths for V2 (1.906 Å) and V3 (1.922 Å). In V^{4+} phosphate structures the bonds are generally at slightly longer distances, but the range overlaps, depending on the particular structure. The PO_4^{3-} groups have regular P−O bonds ranging from 1.514(6) to 1.550(6) Å and bond angles from 102.6(3)° to 112.5(5)° with an average of 109.5°. P−O−V angles are in the range from 130.8(6)° to 137.9(4)°. However, the VO_6 octahedra are distorted because of the difference in bond lengths of the short V═O group versus the long V−OH_2. Consequently, the bond angles between vanadyl oxygen−vanadium and the oxygens in the equatorial plane are larger (99.0° average) than those for water−vanadium and these oxygens (average 81.0°). Thus, the V atom sits above the equatorial plane on the side of the vanadyl oxygen.

(19) Tietze, H. R. *Aust. J. Chem.* **1981**, *31*, 2035.

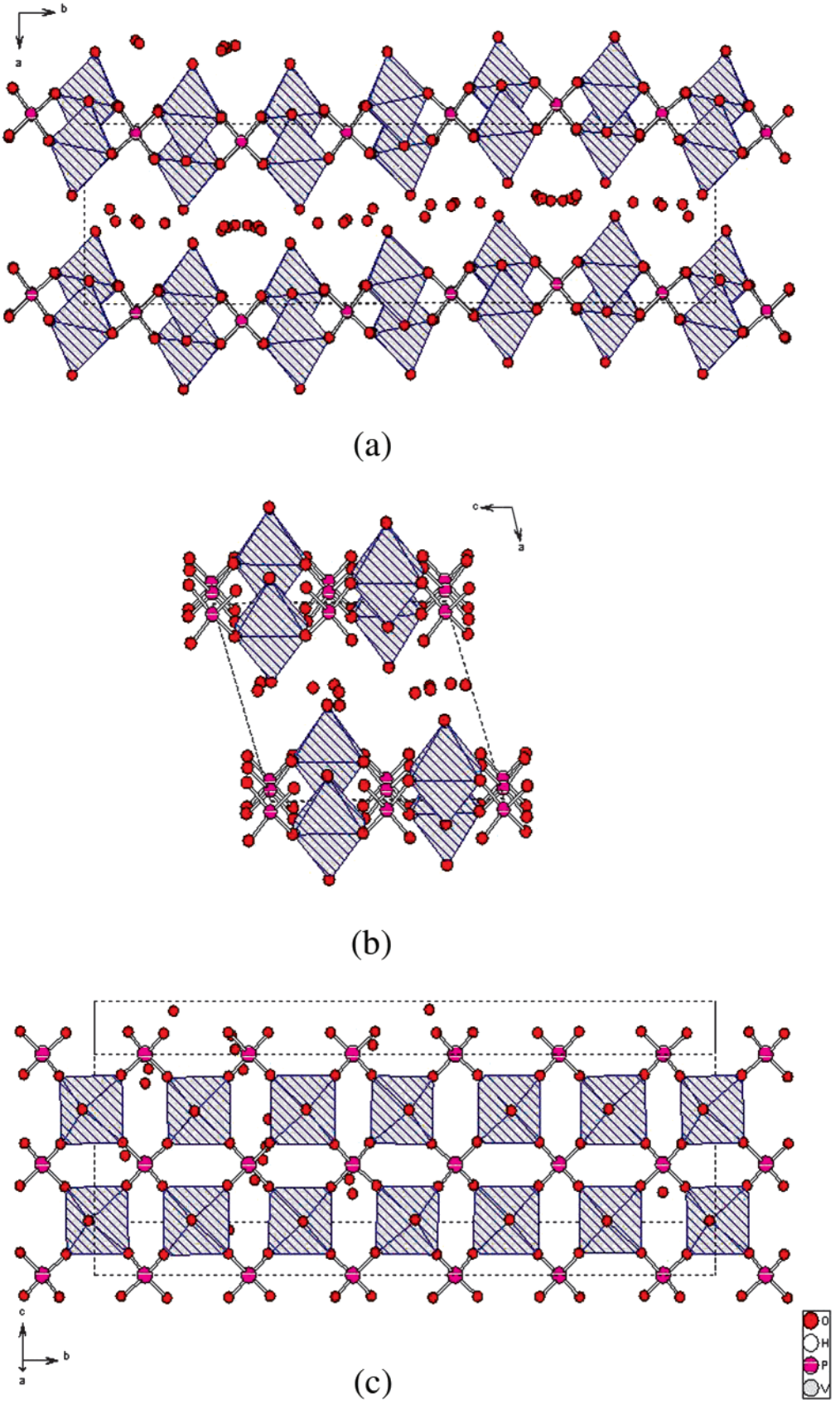

Figure 2. Polyhedral representation of VO_6 octahedra and ball-and-stick representation of PO_4 tetrahedra; (a) a view down the *c* axis showing the curvature of the layers and the positioning of the disordered water molecules between the layers; (b) a view down the *b* axis; and (c) a top view of the layer (perpendicular to the *bc* plane).

The same distortion is true for all the vanadium octahedra. An ORTEP drawing of two octahedra and their connecting tetrahedron are shown in Figure 3.

We have formulated the green phase as $H_xVOPO_4\cdot 2.33H_2O$ because the EPR and NMR results (see below) suggest that some of the vanadium atoms are reduced

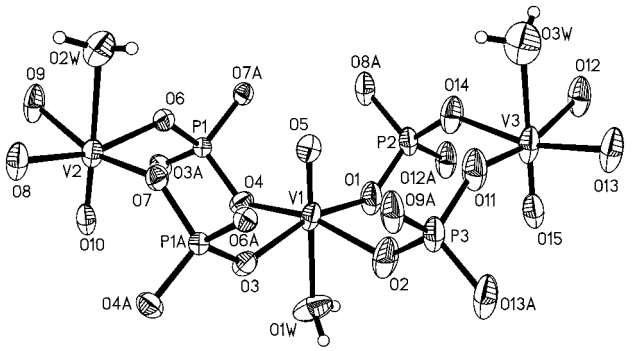

Figure 3. ORTEP drawing of a portion of the layer of the dark green vanadyl phosphate showing the thermal ellipsoids (50% level), the connectivity, and the numbering scheme used in Table 2.

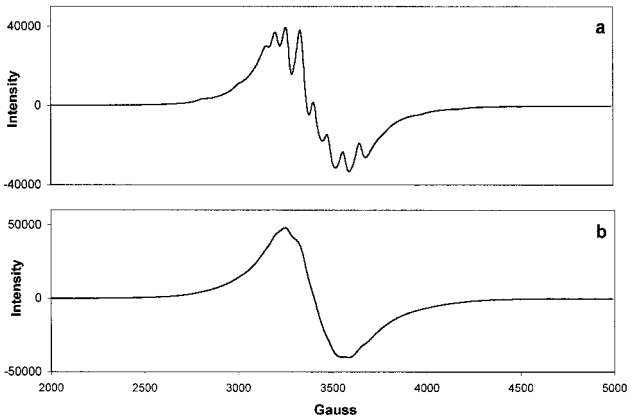

Figure 4. Electron paramagnetic resonance spectra of the light green vanadyl phosphate (a) and the dark green vanadyl phosphate phase (b).

to the +4 oxidation state. In terms of the crystallography the unit cell contains four trimer units $[H(VO)_3(PO_4)_3(H_2O)_3]\cdot 4H_2O$. Titration of samples of the dark green vanadyl phosphate by the standard redox (Ce(IV)−Fe(II)) method yielded V(IV) values from 17 to 22 mol % or an average of 20 mol %. Thus, the formula may be represented as $[H_{0.6}(V^{(IV)}O)_{0.6}(V^{(V)}O)_{2.4}(PO_4)_3(H_2O)_3]\cdot 4H_2O$.

Electron Paramagnetic Resonance. Although V(V) is expected to be an EPR silent species, there is often a small amount of V(IV) present, giving rise to an EPR signal.[21,22] The EPR spectra for both α-$VOPO_4$ and $VOPO_4\cdot 2H_2O$ have been reported.[23,24] It was therefore of interest to see the contrast in EPR spectra of the light green and dark green phases and their comparison to those of $VOPO_4\cdot 2H_2O$.

The spectrum for the light green product is shown in Figure 4a. The vanadium atoms give rise to a weak EPR signal exhibiting hyperfine structure ($V = 7/2$ nucleus). The poor resolution of the hyperfine peaks (inhomogeneous line broadening) is due to the anisotropy caused by the oriented, short V═O bond in the structure.[25] The dark green compound, in contrast, gives rise to a stronger signal that contains no hyperfine structure (Figure 4b). The lack of hyperfine structure in EPR signals of V(IV) phosphates has been attributed to a combination of inhomogeneous line broadening and exchange coupling.[26,27] The fact that a hyperfine structure is not visible in the dark green compound suggests that the V(IV) centers are sufficiently close to one another (<5 Å)[28] to allow exchange coupling to take place. Samples exhibiting line broadening due to magnetic dipole−dipole interactions will sometimes retain hyperfine structure.[25] This indicates a higher density of V(IV) centers in the dark green compound than in the light green compound, in which the hyperfine structure is still discernible.

FT-IR Spectroscopy. A number of FTIR studies of yellow $VOPO_4\cdot 2H_2O$ have been published.[5,23,29] The focus of some of these studies has been the location of the noncoordinated H_2O molecule, which is difficult to determine crystallographically. All report vibrations due to the host lattice in the range 600−1200 cm^{-1}; however, there are some discrepancies in the assignments of the bands. Generally speaking, antisymmetric PO_4^{3-} stretching vibrations occur in the range 1000−1200 cm^{-1}; V═O stretching vibrations occur in the region 980−1040 cm^{-1}; and symmetric PO_4^{3-} stretching vibrations occur around 800−970 cm^{-1}. Some researchers have designated a band at around 1035 cm^{-1}, found also in anhydrous $VOPO_4$, as a PO_4^{3-} antisymmetric stretching vibration. However, the vibration is still present in Raman spectra (in which the antisymmetric PO_4^{3-} stretching vibration is inactive) of both yellow $VOPO_4\cdot 2H_2O$ and our light green compound. This suggests that this vibration, along with a vibration at 995 cm^{-1}, should be attributed to V═O stretching. The authors who conducted the Raman study claim that the vibration at 1035 cm^{-1} indicates the presence of anhydrous $VOPO_4$.[29]

The FTIR spectrum of the dark green compound is presented in Figure 5. Vibrations at 1164 and 1077 cm^{-1} are attributed to antisymmetric PO_4^{3-} stretching. The peak at 1027 cm^{-1} could be an antisymmetric PO_2^{3-} stretching vibration, but more likely it is a V═O stretch in which the coordinated H_2O molecule is missing. There are two rather weak peaks at 1002 and 979 cm^{-1}, which may also be attributed to V═O stretching, but with a coordinated H_2O molecule trans to the V═O bond. In studies of $VOPO_4\cdot 2H_2O$, usually only one V═O stretch for the H_2O- -V═O group is reported. FTIR studies of layered V(IV) phosphate structures with similar V═O units report the stretching vibrations in the range 970−990 cm^{-1}, slightly lower values than those in the V(V) phosphates.[30] The FTIR spectrum of the light green product resembled that of the yellow compound more than the dark green compound, in that only one H_2O- -V═O stretch was observed, but the peaks were poorly resolved.

(20) Tachez, M.; Theobald, F.; Bernard, J.; Hewat, A. W. *Rev. Chim. Miner.* **1982**, *19*, 291.
(21) Cotton, F. A.; Wilkinson, G. *Advanced Inorganic Chemistry*, 5th ed.; John Wiley: New York, 1988; p 688.
(22) Niwa, M.; Murakami, Y. *J. Catal.* **1982**, *76*, 9.
(23) R'Kha, C.; Vandenborre, M. T.; Livage, J.; Prost, R.; Huard, E. *J. Solid State Chem.* **1986**, *63*, 202.
(24) Jordan, B.; Calvo, C. *Can. J. Chem.*, **1973**, *51*, 2621.
(25) Takashi, H.; Shiotani, M.; Kobayashi, H.; Sohma, J. *J. Catal.* **1969**, *14*, 134.
(26) Brückner, A.; Wolf, G. U.; Meisel, M.; Stösser, R. *Eur. J. Solid State Inorg. Chem.* **1993**, *30*, 801.
(27) Brückner, A.; Kubias, B.; Lücke, B. *Catal. Today* **1996**, *32*, 215.
(28) Abragam, A.; Bleaney, B. *Electron Paramagnetic Resonance of Transition Ions*; Clarendon Press: New York, 1970.
(29) Trchová, M.; Čapková, P.; Matějka, P.; Melánová, K.; Beneš, L.; Uhlířová, E. *J. Solid State Chem.* **1999**, *148*, 197.
(30) Amorós, P.; Ibáñez, R.; Martinez-Tamayo, E.; Beltrán-Porter, A.; Beltrán-Porter, D.; Villeneuve, G. *Mater. Res. Bull.* **1989**, *24*, 1347.

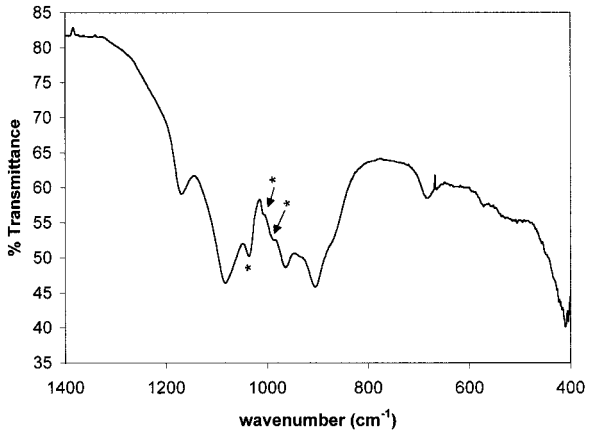

Figure 5. FTIR spectrum of the dark green vanadyl phosphate phase. Bands at 1027, 1002, and 979 cm^{-1} (marked with *) represent V═O stretching vibrations.

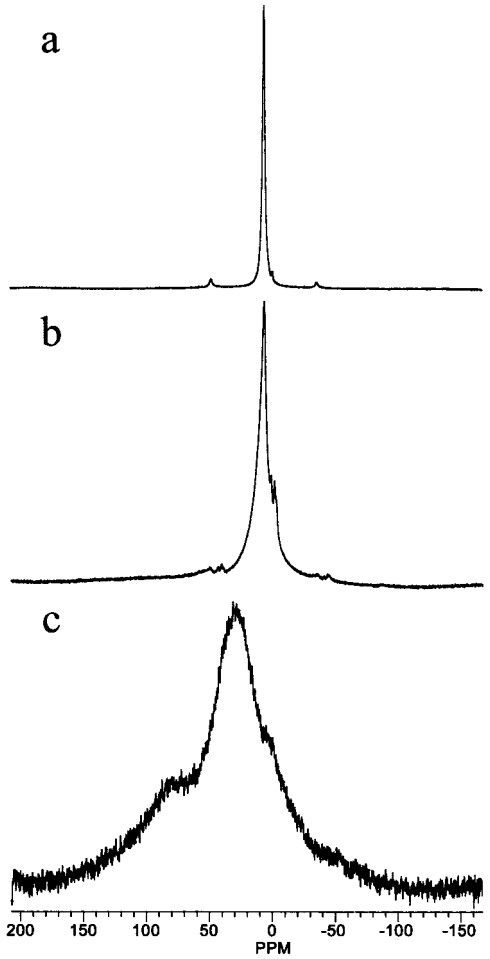

Figure 6. ^{31}P MAS NMR spectra of (a) yellow $VOPO_4\cdot 2H_2O$, (b) the light green vanadyl phosphate phase, and (c) the dark green phase.

^{31}P MAS NMR. ^{31}P MAS NMR spectra of the yellow, light green, and dark green compounds are shown in Figure 6. The spectrum for yellow $VOPO_4\cdot 2H_2O$(a) contains a peak at $\delta = 6.67$ ppm, with one pair of spinning sidebands, and a small peak at $\delta = -0.35$ ppm, which is probably due to free PO_4^{3-} ion present as an impurity (perhaps because the samples were not rinsed with H_2O to remove residual H_3PO_4). The relaxation time was much faster for these samples (3 μs or less instead of 15 μs) than in the H_3PO_4 standard, indicating an interaction between the phosphorus and the vanadium through the connecting oxygen atoms. The spectrum for the light green compound (b) resembles that of the yellow $VOPO_4\cdot 2H_2O$, in that it also contains a peak at $\delta = 6.60$ ppm; however, it is noticeably broader. There is a smaller peak at $\delta = 0.85$ ppm, also probably due to free PO_4^{3-} ions, and another weaker peak at $\delta = -1.92$ ppm. The spinning sidebands appear to be present for all three, but are not so well resolved.

The data for the dark green compound (c) are significantly different than the spectra for either the yellow or the light green compounds. An extremely broad peak is observed at $\delta = 31.49$ ppm, which has two poorly resolved shoulders—one close to 0 ppm and the other $\delta = 78.84$ ppm. The ^{31}P MAS NMR spectra of V(IV) phosphates reveal comparable features, but at very large chemical shifts ($\delta = 1000-3000$ ppm and a peak at $\delta = \approx 0$ ppm).[31]

Thermogravimetric Analysis. Thermogravimetric analyses of yellow $VOPO_4\cdot 2H_2O$ and the dark green compound yield relatively simple weight loss curves. The yellow $VOPO_4\cdot 2H_2O$ shows two fairly sharp steps. The first transition begins almost immediately and corresponds to the loss of the noncoordinated water molecule in the gallery; the second transition, the loss of the coordinated water, begins at about 90 °C and is complete at 180 °C (predicted weight loss, 18.2%; observed, 18.5%). The TGA for the dark green sample also has two steps beginning below 200 °C. However, the first break in the curve occurs at 145 °C and corresponds to a weight loss of 12.9%, equivalent to the loss of 1.5 mol of water/$VOPO_4$ unit. A second weight loss (6.7%) in the temperature range 150−250 °C corresponds to the loss of an additional 0.75 mol of water. A first-derivative plot reveals a third, small weight loss of 1.42%, ending by 350 °C and corresponding to an additional 0.16 mol of water. The total weight loss to 500 °C is 21.8% versus a calculated value of 20.6% for a loss of 7 mol of water in the formula $[H_{0.6}(VO)_3(PO_4)_3(H_2O)_3]\cdot 4H_2O$ [FW = 612.45] or $[H_{0.2}VOPO_4\cdot 2.33H_2O]_3$. There is an additional weight loss of about 3.4% above 750 °C in which the vanadyl phosphate is converted to the pyrophosphate $(VO)_2P_2O_7$. The overall reaction is

$$[H_{0.6}(VO)_3(PO_4)_3(H_2O)_3]\cdot 4H_2O \rightarrow 1.5(VO)_2P_2O_7 + 7.3H_2O + 0.6O_2$$

The total calculated weight loss is 24.60% compared to an observed value of 24.1%.

Phase Interconversion. A fresh sample of yellow $VOPO_4\cdot 2H_2O$ was ground, embedded in glass fiber filter paper through an aerosol chamber, and its powder X-ray diffraction pattern recorded. This procedure drastically reduces the preferred orientation of the sample. It was then allowed to age slowly (Figure 7). After 2 weeks, the X-ray pattern began to exhibit a reflection at $d = 7.12$ Å, in close proximity to the 001 reflection of the yellow phase $d = 7.42$ Å. After 6 weeks, the intensity of the peak at $d = 7.12$ Å had increased until it was nearly equal to the 001 reflection. Additional peaks appeared that could be indexed as belonging to the dark green

(31) Villeneuve, G.; Suh, K. S.; Amorós, P.; Casañ-Pastor, N.; Beltrán-Porter D. *Chem. Mater.* **1992**, *4*, 108.

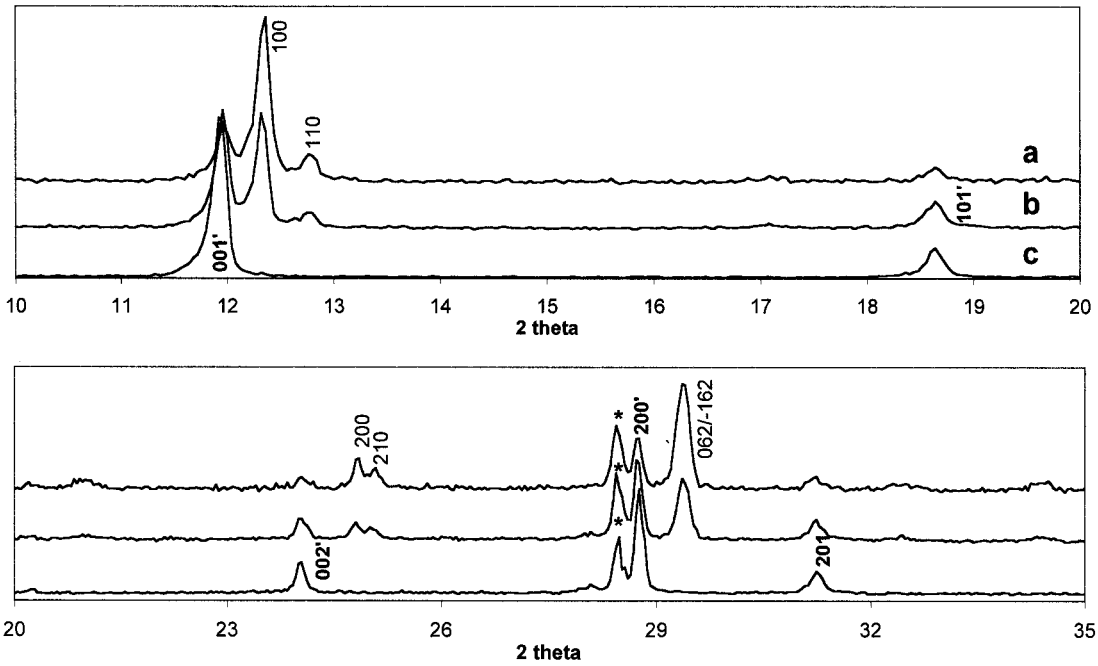

Figure 7. XRPD patterns of the initial yellow $VOPO_4 \cdot 2H_2O$ phase (c), after 6 weeks (b), and after 3.5 months (a), when the slow conversion to the dark green $[H(VO)_3(PO_4)_3(H_2O)_3] \cdot 4H_2O$ is nearly complete. Indices written as (100) etc. represent features of the dark green phase. Indices written as (001′) represent features of the yellow phase. Peaks marked with (*) are from a Si standard.

$H_{0.2}VOPO_4 \cdot 2.33H_2O$ ($d = 7.06$ Å from the single-crystal data). After 3.5 months, the pattern consisted mainly of peaks belonging to $H_{0.2}VOPO_4 \cdot 2.33H_2O$. During the summer, the conversion occurred more rapidly, reaching completion in 6 weeks. The results suggest that yellow $VOPO_4 \cdot 2H_2O$ converts to dark green $H_{0.2}VOPO_4 \cdot 2.33H_2O$ with time and that the light green product is really just a mixture of the two phases.

Synthesis. Initially, yellow, light green, and dark green products were synthesized under virtually the same experimental conditions, namely, those described in the synthesis of the light green product. Later, the syntheses were optimized such that they favored the formation of one product over the others. The yellow phase is best synthesized with short reaction times at lower temperatures in the presence of an oxidizing agent. We have found that the addition of a small amount of nitric acid is very effective in the prevention of V(IV) formation. Longer heating time, more concentrated solutions, and increasing H_3PO_4 content seem to favor the reduction of the vanadium, resulting in the formation of $H_{0.2}VOPO_4 \cdot 2.33H_2O$. However, the best procedure is to use a specific amount of reducing agent. Ethanol was used as a reducing agent in the preparation of a series of $Na_xVOPO_4 \cdot 2H_2O$ phases with various amounts of Na^+.[9b] Addition of excess ethanol, however, leads to the formation of $VO(HPO_4) \cdot 0.5H_2O$.[32]

Porous Products. The first step in preparing porous products from the dark green vanadyl phosphate is to spread the layers apart by amine intercalation. Intercalation of hexylamine in alcohol leads to an interlayer spacing of 18.4 Å. In reaching the final intercalate composition of slightly less than 2 mol of amine/vanadium, the solution is colorless, while the solid becomes dark blue-green, blue-grey, and finally bluish-white in the process. Apparently, the end product is a colorless V(V) product, resulting from a redox reaction. This sequence of reactions is under investigation and will be reported upon subsequently.

Table 3. Elemental Composition of the Vanadyl Phosphate Pillared with Nickel Species

solvent sample ID	P, %	Ni, %	V, %	C, %	H, %	N, %
methanol III-71B	8.73 (2.05)[a]	23.07(2.86)	6.99	18.77	5.24	3.46
propanol III-72B	9.53 (1.99)	21.92(2.42)	7.87	17.06	5.03	3.14
heptanol III-72C	8.21 (2.21)	22.77(3.23)	6.12	19.86	5.38	2.95

[a] Values in parentheses show the number of respective mol/mol of vanadium.

Table 4. Pore Size Characterization (MP Method) of the Nickel Pillared Vanadyl Phosphate versus Calcination Temperature

sample ID	BET surface area/ *t*-method micropore area (m^2/g)						pore size (Å)	
	260 °C		406 °C		500 °C		226 °C	406 °C
III-71B	215.0	209.8	117.7	112.6	6.2	–	6.9	11.7
III-72B	185.0	179.6	131.7	125.6	18.0	–	10.9	13.1
III-72C	401.9	387.2	286.3	236.0*	52.8	–	16.1	22.4

The addition of excess amine, followed by the addition of the alcohol−water mixture, resulted in gel formation, which was refluxed to obtain the porous product. Elemental analysis of the nickel−vanadyl phosphate composite products, obtained in different alcohols as solvent, are shown in Table 3 and texture qualities in Table 4. The N_2 BET isotherms are shown in Figure 8. Surface areas and pore size measurements, presented in Table 4, were obtained from the N_2 BET isotherms using the t-plot method.[33] Calcination at 260 °C removes

(32) Johnson, J. W.; Johston, D. C.; Jacobson, A. J.; Brady, J. F. *J. Am. Chem. Soc.* **1984**, *106*, 8123.

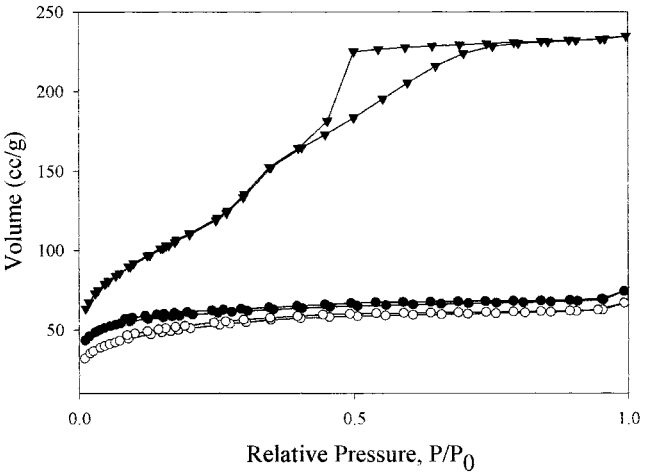

Figure 8. Nitrogen sorption−desorption isotherms for the nickel acetate treated vanadyl phosphates prepared in methanol (filled circles), propanol (open circles), and heptanol (filled triangles) precalcined at 260 °C.

all the amine and solvent, yielding high surface area products. We note a trend toward higher surface areas and pore sizes with an increase in the chain length of the alcohol solvent. In fact, the isotherm for sample III-72C is of a totally different type from the samples prepared in the smaller size alcohols. We also observe a trend to larger pore sizes with an increase of calcination temperature.

Another feature of the porous products is the low amount of vanadium, something of the order of half the phosphate content. Yet the layered nature of the products was maintained as shown by SEM photographs. The loss of vanadium may well result from the excess of added amine in the reaction mix.

Sample 59C, prepared in propanol as a solvent, when calcined at 324 °C exhibited a Type I isotherm with a surface area of 346 m^2/g of which the area due to micropores was 343 m^2/g. This sample yielded a single-peak X-ray pattern, $d = 27$ Å. Its micropore volume was 0.152 cm^3/g with the pore size distribution shown in Figure 9a. When the sample was heated to 414 °C, the surface area decreased to 146 m^2/g with a narrow pore size distribution centered at 20-Å diameter (Figure 9b).

Discussion

During the revision of this paper, it came to our attention that the dark green vanadyl phosphate had been reported earlier, but with no crystal structure solution.[34] It was prepared by reduction of the yellow $VOPO_4\cdot 2H_2O$ with hydroquinone. The formula was given as $H_xVOPO_4\cdot 2.33H_2O$, and for $x = 0.2$, the interlayer spacing was reported to be 7.0 Å compared to our value of 7.06 Å. In our case, the reductant was alcohol under hydrothermal conditions. The very slow reduction of the yellow vanadyl phosphate upon standing in air may be the result of residual organic contacting the crystals. When nitric acid was used in the preparation of the yellow phase, no reduction was observed during the preparation or upon storing. The addition of alcohol in the place of HNO_3 ensured that the green phase would form.

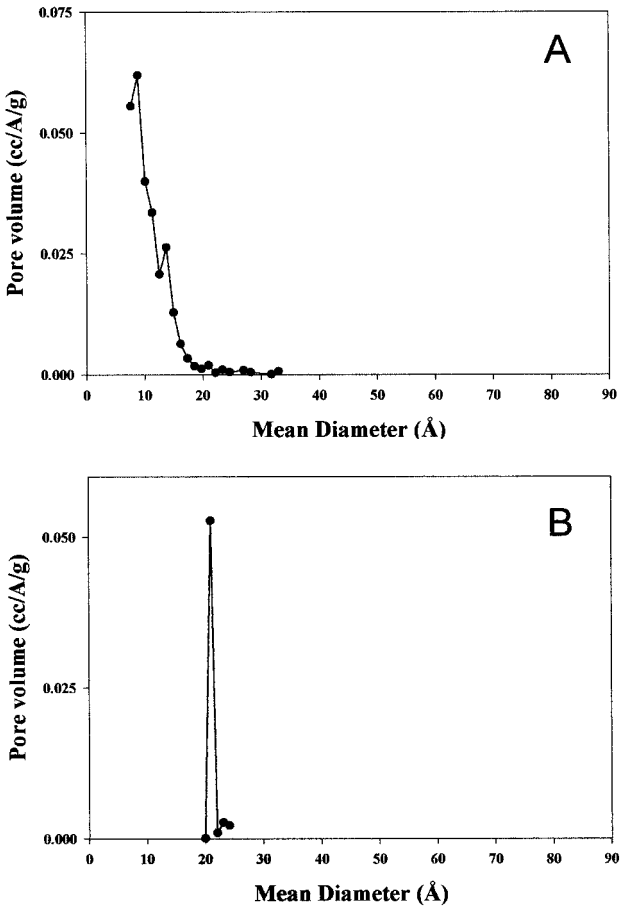

Figure 9. (a) Pore volume versus mean diameter plot for the nickel−vanadium phosphate showing a bimodal pore distribution (9 and 13 Å) for the product heated at 324 °C. (b) Pore volume versus mean diameter plot for the nickel−vanadium phosphate, reheated to 414 °C. The pore distribution narrows and shifts to ≈20 Å.

The structures of the yellow and green phases are related. The cell dimensions of the yellow vanadyl phosphate are $a = 6.202$ Å and $c = 7.410$ Å with space group $P4/mmm$. In the green phase, the b axis is $\sqrt{2}\cdot 3a$ and the c axis is $(\sqrt{2})a$, where a is the 6.202-Å unit cell dimension. This means that the alternation of octahedra and tetrahedra in the green phase parallels that along the ab diagonal of the yellow phase.

Intercalation of metal ions by interaction of metal oxides, MI, where M is an alkali metal, with $VOPO_4\cdot 2H_2O$ yielded a green, reduced vanadium phase.[34,35] The reported interlayer spacings are smaller than 7 Å, indicating a tighter binding of the layers. According to Ayyappan,[36] several metal intercalated layered vanadyl phosphates possess structures derived from $VOPO_4\cdot 2H_2O$. A full discussion of the variance in the many structures cited is presented in his dissertation.

More recently, Jacobson et al.[37] obtained $(NH_4)VOPO_4\cdot 1.5H_2O$ and $(NH_4)_{0.5}VOPO_4\cdot 1.5H_2O$. These authors examined the system $V_2O_5-H_2C_2O_4-H_3PO_4-NH_4OH$. In the production of the ammonium vanadyl

(33) Gregg, S. J.; Sing, K. S. W. *Adsorption, Surface Area Porosity*, 2nd ed.; Academic Press: New York, 1982.
(34) Jacobson, A. J.; Johnson, J. W. *Mater. Sci. Monogr.* **1985**, *28A*, 469.
(35) Johnson, J. W.; Jacobson, A. J. *Angew. Chem., Int. Ed. Engl.* **1983**, *22*, 412.
(36) Ayyappan, P. Ph.D. Dissertation, Indian Institute of Technology, Delhi, India, Sept 1999; p 11.

phosphates, the oxalic acid acted as a reducing agent, but under other conditions oxalic acid also complexed the vanadium. Red crystals of NH_4VOPO_4[38] were obtained as a byproduct of the synthesis of the half-ammonium salt. None of the compounds cited above match the vanadyl phosphate reported here. However, $(NH_4)_{0.5}VOPO_4 \cdot 1.5H_2O$ is monoclinic $P2_1/m$ with a = 6.9669(6) Å, b = 17.663(2) Å, c = 8.9304(8) Å, and β = 105.347(1)°. The layers are quite similar in the arrangement of the tetrahedra and octahedra and their puckered nature to that of the dark green compound reported here. There are three distinct V−O octahedra with the vanadyl oxygen trans to the vanadium-bonded water molecule. The average oxidation state of V is 4.5. These authors attribute the puckered nature of the layers to the unequal equatorial V−O bonds. In fact, they average 2.028 for V1, 1.895 for V2, and 1.960 Å for V3 in $(NH_4)_{0.5}VOPO_4 \cdot 1.5H_2O$ as compared to 1.963, 1.906, and 1.922 Å in our dark green phase.

The study carried out by El Haskouri et al.[13] provides clues as to how porous materials may result from the gel technique. Because they carried out their reaction at a pH value close to 1.2, the species in solution was considered by them to be sheets of $[VOPO_4]^{n-}{}_m$. These lamellae are flexible enough to twist around the template micelle that then aggregate to form the hexagonal mesoporous product. The mechanism is similar to S^+I^- charge density matching[39] where the template micelle charge neutralizes the layer negative charge.

In the porous products described in this paper, the reaction was carried out in basic solution (excess amine). Under these conditions we have found, in separate experiments with the dark green amine intercalates, that they become white. However, they retain the amine and exhibit a large interlayer spacing. The removal of color indicates the oxidation of V(IV) to the +5 state and neutral layers. The hexylamine template is also neutral. The end product contained about 1.8 mol of amine/mol of vanadium, compared to a ratio in excess of 5:1 in the reaction mixture. In addition, a small amount of acetate species may be retained as the amount of carbon present was somewhat in excess of that required for the presence of the hexylamine. Thus, we conclude that the amine acts as a neutral template to form a mixed nickel vanadium phosphate with a microporous structure. When the vanadyl phosphate is omitted from the reaction mix, the nickel acetate $(NH_4)_2HPO_4$ mixture does not produce microporous products. Thus, the vanadyl phosphate is essential in these reactions and its role, as well as the nature of the intermediates, will be probed in future studies.

Our further investigations will focus on how the lamellar material is able to retain its layered structure and form relatively narrow pore sizes that increase in pore size at higher temperature, retaining the narrow pore size distribution.

Acknowledgment. This study was supported by the National Science Foundation, under Grants DMR-9707151 and DMR-0080040, for which grateful acknowledgment is made.

Supporting Information Available: Tables listing atomic positional parameters and isotropic thermal parameters of the non-hydrogen atoms, a complete table of bond distances and angles, anistropic thermal parameters of the non-hydrogen atoms, positional parameters for H atoms, and possible hydrogen bonds (PDF). This material is available free of charge via the Internet at http://pubs.acs.org.

CM0008821

(37) Do, J.; Bontchev, R. P.; Jacobson, A. J. *Inorg. Chem.* **2000**, *39*, 3230.

(38) Haushalter, R. C.; Chen, Q.; Soghomonian, V.; Zubieta, J.; O'Connor, C. J. *J. Solid State Chem.* **1994**, *108*, 128.

(39) Huo, Q.; Margolese, D. I.; Ciesla, U.; Feng, P.; Gier, T. E.; Sieger, P.; Leon, R.; Petroff, P. M.; Schueth, F.; Stucky, G. D. *Nature* **1994**, *368*, 317.